

Automated Ovarian Cancer Identification Using End-to-End Deep Learning and Second Harmonic Generation Imaging

Guangxing Wang, Huiling Zhan, Tianyi Luo, Bingzi Kang, Xiaolu Li, Gangqin Xi,
Zhiyi Liu[✉], and Shuangmu Zhuo[✉]

Abstract—Surgery is one of the most important methods for the treatment of ovarian cancer. During this procedure, a biopsy is usually required to evaluate the suspicious lesions and provide guidance for the size of the surgical resection. However, the conventional biopsy for intraoperative histopathological diagnosis performed by trained pathologists is labor-intensive, time-consuming, and carries the risk of bias. Therefore, we present a novel optical biopsy method to assist physicians in accurately and rapidly diagnosing ovarian cancer during surgery. We demonstrate that second harmonic generation (SHG) images of unstained, freshly resected ovarian tissues can be accurately characterized by deep learning techniques. Using 13,563 SHG images obtained from freshly resected human ovarian tissues of 74 patients, we fine-trained a convolutional neural network (CNN) based on pretrained ResNet50 framework to distinguish normal, benign, and malignant ovarian tissue with an average accuracy of 99.7%. These results suggest that optical biopsies based on label-free SHG imaging and deep learning technology have great potential for rapid and accurate characterizations of ovarian lesions in surgery.

Index Terms—Deep learning, optical biopsy, ovarian cancer, second harmonic generation imaging (SHG).

Manuscript received 26 September 2022; revised 7 December 2022 and 8 December 2022; accepted 8 December 2022. Date of publication 12 December 2022; date of current version 23 December 2022. This work was supported in part by the National Key Research and Development Program of China under Grant 2019YFE0113700, in part by the Natural Science Foundation of Fujian Province under Grant 2021J01431 and 2022J01340, and in part by the Joint Funds of Fujian Provincial Health and Education Research under Grant 2019-WJ-21. (*Corresponding authors:* Shuangmu Zhuo; Zhiyi Liu.)

This work involved human subjects or animals in its research. Approval of all ethical and experimental procedures and protocols was granted by Affiliated Cancer Hospital of Fujian Medical University.

Guangxing Wang is with the School of Science, Jimei University, Xiamen 361021, China, and also with the State Key Laboratory of Molecular Vaccinology and Molecular Diagnostics, Center for Molecular Imaging and Translational Medicine, School of Public Health, Xiamen University, Xiamen 361102, China (e-mail: awanggx@126.com).

Huiling Zhan, Tianyi Luo, Bingzi Kang, Xiaolu Li, Gangqin Xi, and Shuangmu Zhuo are with the School of Science, Jimei University, Xiamen 361021, China (e-mail: 310088276@qq.com; 2651485278@qq.com; 845991423@qq.com; lixiaolu@jmu.edu.cn; xigangqin@jmu.edu.cn; shuangmuzhuo@gmail.com).

Zhiyi Liu is with the State Key Laboratory of Modern Optical Instrumentation, College of Optical Science and Engineering, International Research Center for Advanced Photonics, Zhejiang University, Hangzhou, Zhejiang 310027, China, and also with the Intelligent Optics & Photonics Research Center, Jiaxing Research Institute, Zhejiang University, Jiaxing 314000, China (e-mail: liuzhiyi07@zju.edu.cn).

Color versions of one or more figures in this article are available at <https://doi.org/10.1109/JSTQE.2022.3228567>.

Digital Object Identifier 10.1109/JSTQE.2022.3228567

I. INTRODUCTION

OVARIAN cancer has the highest mortality rate among all gynecologic tumors and seriously threatens the health of women worldwide [1]. In general, ovarian cancer can be categorized as benign and malignant forms according to its biological behavior and effects on the body. Benign tumors are usually well differentiated, have low atypia, grow slowly, and have little impact on the body, are easily treated, and have a relatively good prognosis. In contrast, malignant tumors are characterized by poor differentiation, severe atypia, rapid growth rate, and great damage to the body, requiring complex treatment procedures and have relatively poor prognosis. Misdiagnosis of a malignant tumor as a benign tumor may lead to undertreatment, and thus preventable deaths [2]. Likewise, if a benign tumor misdiagnosed as a malignant tumor, it may lead to excessive treatment, which resulting in unnecessary side effects and additional treatment costs [3]. Therefore, the importance of accurate diagnosis in formulating optimal treatment and prognosis for patients cannot be underestimated. Currently, histopathological analysis is the “gold standard” for making an unequivocal diagnosis in the clinic [4]. However, conventional histopathological examination requires tissue fixation, embedding, sectioning, and staining, and patients usually require 1-3 days to receive the diagnostic report. In addition, this process is time-consuming and laborious, and may lead to inter-observer errors, which affects the rapid diagnosis of patients and the determination of the treatment plan during surgery [5], [6]. Rapid and accurate diagnostic analysis of patients during surgery can determine the size of surgical resection, improve patients’ prognosis, avoid re-operation, and reduce costs [7], [8]. In addition, rapid and accurate intraoperative diagnostic analysis can provide valuable information for determining drug administration during surgery in some situations [9]. Currently, fresh frozen sectioning (FFS) is the standard for intraoperative surgical examination [10]. Although intraoperative diagnosis of ex vivo biopsy is relatively fast, FFS still requires nearly one hour. What’s more, the quality of tissue sections is often compromised by freezing and section, which affects the accuracy of diagnosis to some extent [11], [12], [13]. Therefore, to improve the efficiency of intraoperative diagnosis and reduce the likelihood of misdiagnosis, it is urgent to develop a new method that enables rapid, non-destructive, accurate, and automatic diagnosis of ovarian cancer patients during surgery.

In recent decades, second harmonic generation (SHG) imaging technology, which is characterized by label-free, nondestructive, and high resolution has been widely used in biology, tissue engineering and disease diagnosis [14], [15], [16], [17]. SHG as a second order coherent process utilizes a long-wavelength near-infrared femtosecond laser source to realize endogenous chromophore excitation, which can perform high resolution deep tissue imaging, reduces phototoxicity, and offers the possibility of long-term imaging [18]. In addition, as one of the main components of the extracellular matrix, collagen fiber plays a certain role in the occurrence and progression of diseases [19], [20]. Therefore, its changes in tissue can be used as an important biomarker for disease diagnosis [21]. Since collagen fibers with their non-centrosymmetric structure supports SHG imaging, they can be observed non-destructively with high resolution SHG imaging technology, which enables rapid, non-destructive, and accurate diagnosis of ovarian cancer.

Nevertheless, the big imaging dataset generated by SHG imaging technology typically require biomedical engineers, biologists, and experienced pathologists to evaluate and provide valuable information for meaningful interpretation and classification. This process is like that of the conventional histopathological examination method, which is also laborious and prone to inter-observer errors [22], [23]. Therefore, since the early 1980s, computer-aided diagnosis methods have been introduced into clinical research and practice to help physicians evaluate and analyze medical images, so as to improve their work efficiency [24]. As one of the emerging computer technologies, machine learning technology has been widely used to detect and diagnose diseases in computer-aided diagnosis system [25], [26]. Conventional machine learning techniques first use a segmentation algorithm to determine the region of interest in the image and then perform feature extraction of the region of interest. Finally, the classification algorithm based on statistics or shallow artificial neural network is used to perform diagnostic analysis of medical images. For example, Torrents-Barrena et.al. used Gabor filters to extract texture information from X-ray images of breast tissue, and then support vector machine was used to classify normal and abnormal tissues. The classification accuracy was as high as 84.86% [27]. In addition, the computer-aided diagnosis models based on radiomics feature extraction methods and machine learning algorithm were constructed to achieve accurate identification of benign, malignant, borderline, and normal ovarian tissues via SHG images with the accuracy over 90% [28], [29]. Unfortunately, conventional machine learning methods require extensive image processing and hand-crafted feature extraction processes, in which each step is not independent. The quality of each process results will affect the next process step. In the end, the final training results are influenced. Moreover, feature extraction as the most important unit of the whole process, based on manual feature engineering, requires domain-specific knowledge and is limited to processing natural data without manual intervention. In comparison, deep learning, a rapidly developing field of machine learning, uses an end-to-end training mode to process datasets, which avoids excessive manual intervention and improves the fit of the computer-aided diagnosis model [30]. Convolutional Neural Networks (CNN), as one of the

deep learning technologies, mimic the biological mechanism of visual perception and have achieved remarkable results in medical image analysis and diagnosis [31], [32]. Each neural layer extracts the information in the original image through convolution, pooling and other operations to create a feature map which is then passed to the next neural layer to finally obtain the corresponding processing results. In this process, the CNN can automatically abstract the representative features from the imported image, avoiding the manual intervention in conventional machine learning. The accuracy and robustness of the computer-aided diagnosis model can be improved, and the results can be comparable with those of experts [33].

Therefore, in this study, we present a new method that combines SHG imaging and deep learning technology to accurately and rapidly classify the different types (normal, benign, and malignant) of human surgical ovarian tissues ex vivo. Based on a transfer learning approach, we fine-tuned the pre-trained CNN by using 13563 SHG images obtained from freshly resected surgical human ovarian tissue of 74 patients. The classification performance of this fine-tuned computer-aided diagnosis model then achieved an average accuracy of 99.7%. These results suggest that our approach is convenient can be used alongside the surgical bed. This holds great promise for rapid and accurate ovarian cancer diagnosis in the clinic and assists doctors in clinical decision-making (Fig. 1)

II. MATERIALS AND METHODS

A. Specimen Preparation

Seventy-four patients from Affiliated Cancer Hospital of Fujian Medical University were recruited for this study with the approval of the Institutional Review Board. Freshly collected ovarian tissues were diagnosed by experienced pathologists, including 26 benign tumor tissues, 23 malignant tumor tissues and 25 normal tissues. In addition, portions of the freshly excised ovarian tissues were retained for SHG imaging. Before SHG imaging, the residual blood was removed with a phosphate-buffered saline, which is also able to prevent tissue shrinkage during imaging. All the samples were sliced with a thickness of approximately 50 μm . After SHG imaging, the imaging areas of ex vivo ovarian tissue were marked and carefully examined by pathologists to verify that the histopathological category of the imaging areas was consistent with the diagnostic result.

B. SHG Imaging

SHG imaging of excised ovarian tissue was performed with a commercial nonlinear optical microscope consisting of a mode-locked Ti:sapphire femtosecond laser with 80-MHz repetition rate and \sim 140-fs pulses (Chameleon Ultra II; Coherent, USA) and confocal laser scanning microscope (LSM 880; Zeiss, Germany). The laser source is linearly polarized. The excitation laser with a wavelength of 810 nm was used and focused on the ex vivo specimen through a plan-apochromat oil immersion objective (63 \times , numerical aperture of 1.4, Zeiss) to relatively reduce the effect of down-sampling in model construction. The laser power

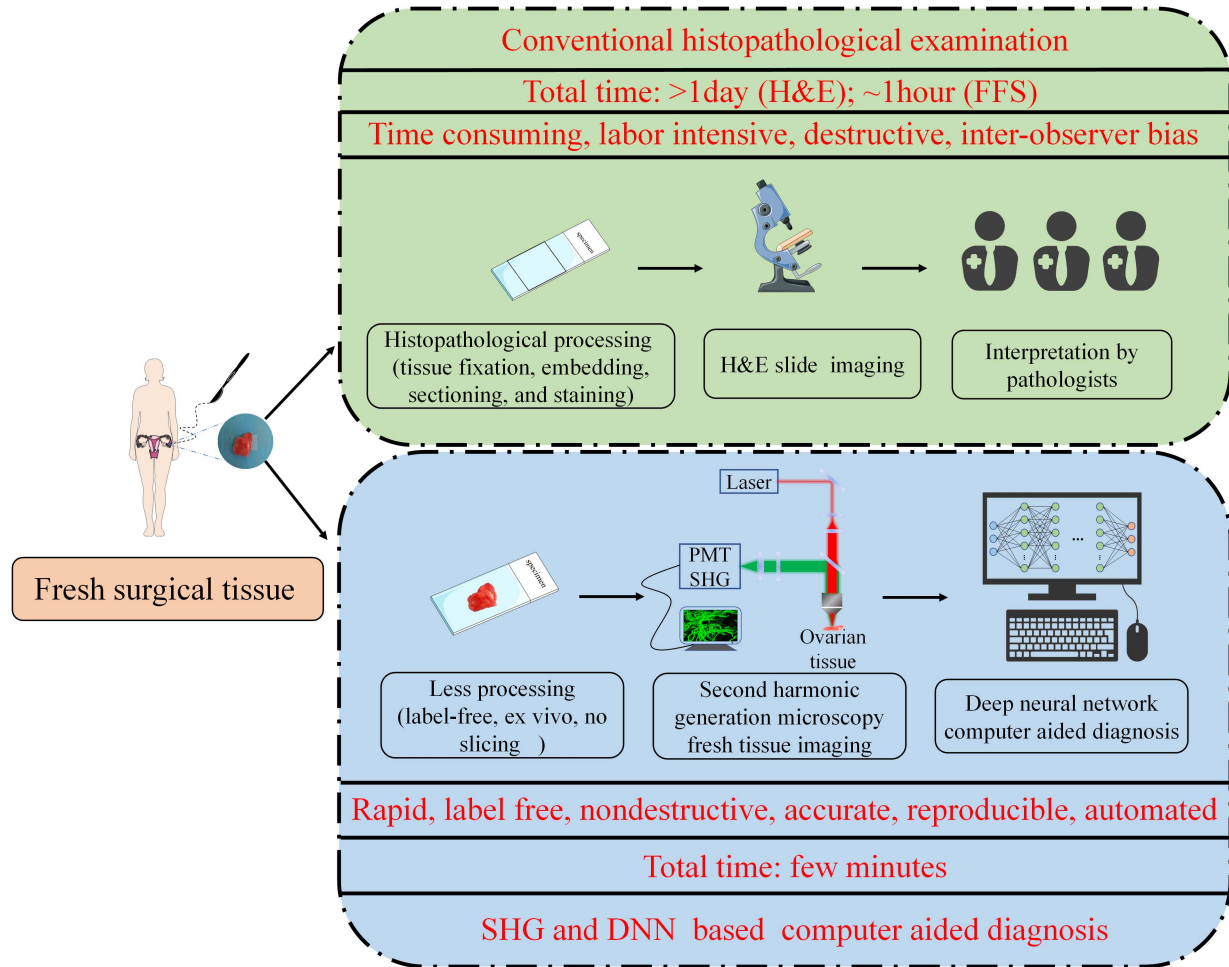


Fig. 1. Workflow of intraoperative ovarian cancer diagnosis using SHG and deep learning. Compared with conventional histopathological examination, the method we proposed in this study requires less tissue processing and could diagnose in real-time based on SHG and deep learning. (H&E, hematoxylin and eosin; FFS, fresh frozen sectioning; SHG, second harmonic generation; PMT, photomultiplier tube; DNN, deep neural network.).

measured at sample was approximately 50 mW. The imaging plane was selected at medially axial position with optimal imaging quality in tissue slice. Subsequently, the backscattered SHG signals were collected with the same objective and detected with a photomultiplier tube filtered from 395 nm to 415 nm without anisotropy measurement, which was then color-coded as green to obtain SHG images of the collagen of the ex vivo specimen. The field-of-view of each SHG image was $134.95 \times 134.95 \mu\text{m}^2$, and contained 512×512 pixels with a data depth of 12 bits (intensity range: 0~4095 grayscale units). Since the pixel dwell time was $2.05 \mu\text{s}$, the acquisition of each SHG image cost only about 0.5 s. To ensure the quality of the training dataset for building the computer-aided diagnosis model, only the lesion area of the ex vivo specimen was acquired.

C. Computer-Aided Diagnosis by CNN

Recently, CNN has been widely used in medical imaging [34], [35]. In principle, it uses a computational model composed of multiple artificial neural network layers, such as convolutional, pooling, activation, and fully connected layers, to extract and learn inherent features in image data. To meet the specific

requirements of different tasks, appropriate CNNs are designed and trained by iteratively optimizing the weights and deviations of the networks to minimize the loss function. Although the use of CNN in medical image analysis has achieved a great success, a large dataset is usually required to optimize the performance of CNN and overcome problems related to overfitting [36]. For example, the well-known CNN based on ResNet50 framework successfully classifies 1000 image categories by training on the ILSVRC-2015 dataset which contains 1.3 million training images, 500000 verification images and 100000 unclassified test images [37]. In contrast, there are no comprehensive SHG image datasets to train the specific CNN for ovarian cancer classification from scratch. Fortunately, transfer learning, a method in which a previously pre-trained model is reused for a different but related task, has been introduced into deep learning to solve the model training problem caused by lack of training data, which has been shown to be effective in training deep learning with a relatively small dataset [38].

Therefore, in this study, we did not train the CNN model for ovarian cancer diagnosis from scratch, but used a pre-trained CNN based on ResNet50 to enable rapid and accurate diagnosis of benign, malignant, and normal ovarian tissue. As shown in

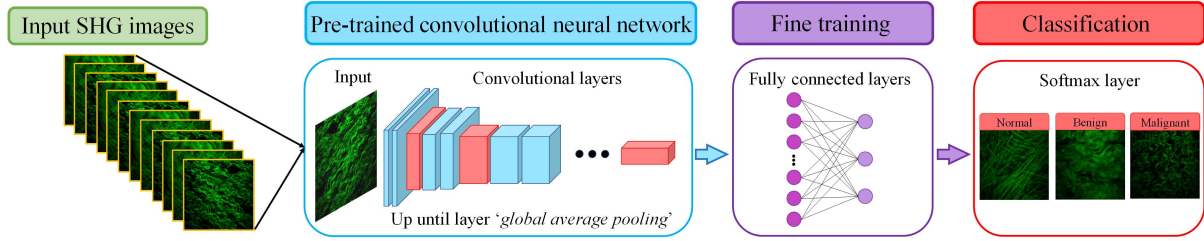


Fig. 2. Schematic diagram of the proposed model based on transfer learning for ovarian cancer diagnosis.

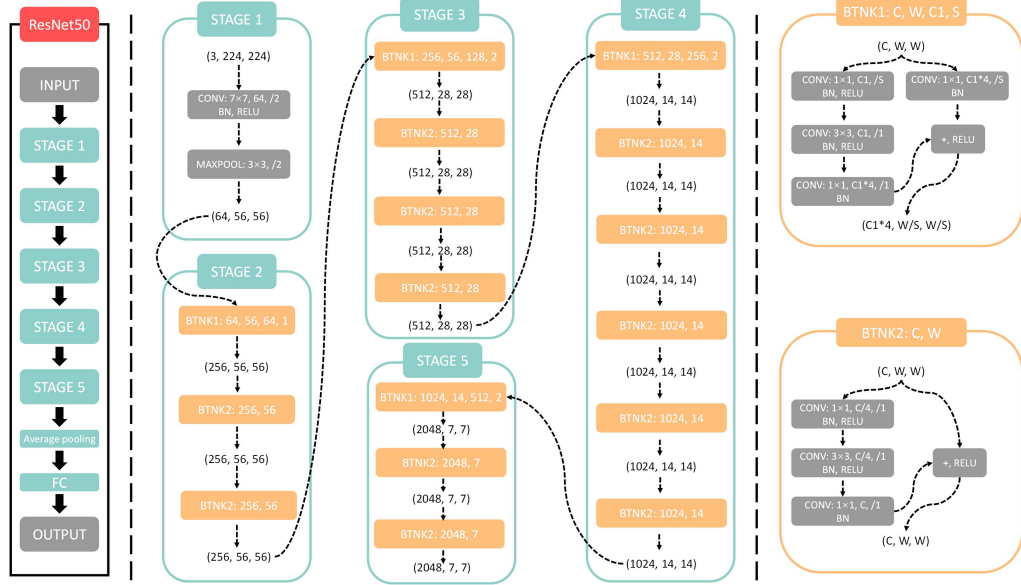


Fig. 3. Illustration of ResNet50 architecture [37]. FC: Fully connected layer. CONV: Convolution. BN: Batch normalization. BTNK1: Bottleneck 1. BTNK2: Bottleneck 2. (C, W, W): (Channel, width, height); considering that the images involved in this model are squared, the width and height of the images are equal. C1: Channel. S: Stride.

Fig. 2, the pre-trained convolutional layers of ResNet50 were kept in the CNN model for ovarian cancer diagnosis. In addition, the fully connected layers of ResNet50 were replaced with a brand new fully connected layer that outputs the final feature representations using the SoftMax activation function to identify different types of ovarian tissues.

Before training the proposed model, several pre-processing steps were performed on the ovarian SHG imaging dataset. Since the primary ovarian SHG imaging dataset, which consisted of 4521 images from 74 patients, was relatively small for better model training, we augmented the dataset by horizontal and vertical flipping, generating a total of 13563 images as the final complete dataset. Subsequently, an independent test set (20% of the final complete dataset) was selected from the final complete dataset. The remaining images were randomly split into a training data set and a validation data set with a ratio of 60/20 in the final complete dataset. The images in the training and test datasets were from different patients, so each patient's images were used in either the training/validation or test dataset but could not be used in both. To meet the input image size requirements in ResNet50, all images were resized to the target size of 224×224 pixels by down-sampling. Then, the pre-processed image dataset

was transferred to proposed ovarian cancer diagnostic model based on the ResNet50 architecture (as shown in Fig. 3) for model training. ResNet50 consists of 16 bottleneck blocks (BTNK) that have skip connections to jump over layers and avoid the vanishing gradient problem. First, the images were input to the model with a batch size of 32. Under transfer learning method, the parameters of the previous convolutional layer are the same as those trained on ImageNet. Next, the feature maps were obtained under the activation function of ReLU after successively processing from STAGE1 to STAGE5. Moreover, the global average pooling layer was used to reduce the spatial size of the feature representation and the number of trainable parameters. Then the reduced feature maps were used as inputs to the brand new fully connected layers for fine-tuning. Then, the SoftMax classification layer was used to classify the feature vectors into three categories of ovarian tissue (benign, malignant, normal) by minimizing the cross-entropy loss function. During the training process, the Adam optimization algorithm with an initial learning rate of 0.0001 was used to optimize the weight and deviation of a brand new fully connected layer. All construction and implementation of the deep learning model was done in MATLAB using the Deep Learning Toolbox.

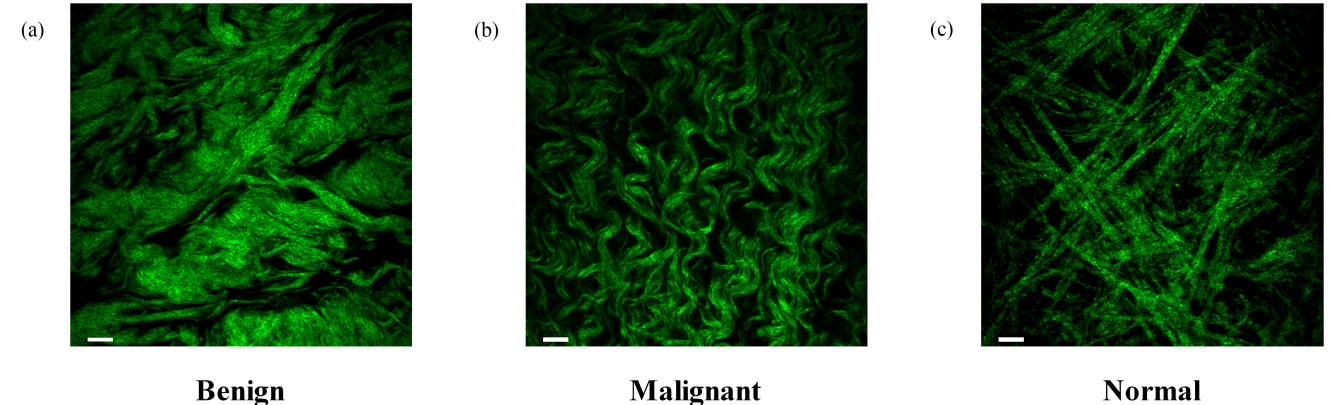


Fig. 4. Representative SHG images of ovarian tissue: (a) Benign, (b) Malignant, and (c) Normal tissue. (Scale bar: 10 μm).

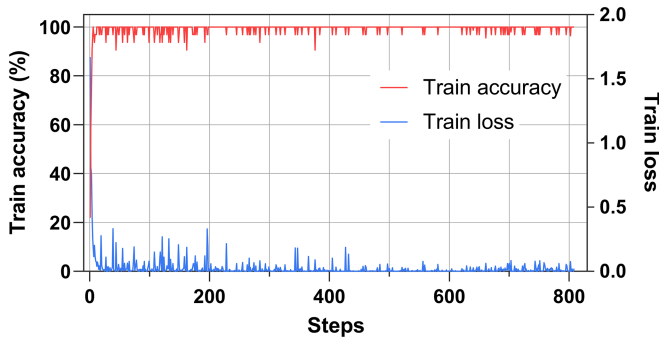


Fig. 5. Training performance of the CNN ovarian cancer diagnostic model in the training dataset.

III. RESULTS

In this study, a total of 4521 SHG images (benign: 1057, malignant: 1507, normal: 1507) were obtained from fresh isolated ovarian tissue without staining. Fig. 4 shows the representative SHG images from the three different ovarian tissue types. As can be seen in Fig. 4, the collagen fibers existing in different types of ovarian tissues have changed significantly in terms of their morphological structure. In normal ovarian tissue, each collagen fiber has a linear form and interlaced structure with no obvious overall directionality. The collagen fibers of malignant ovarian tissue have a wavy form, which has a certain direction. In contrast, the collagen fibers in benign ovarian tissue are denser and more curved, with more aggregation and no directivity. In conclusion, these results confirm that the morphology and structure of collagen fibers in the extracellular matrix of ovarian tissue changes when the cells become cancerous, which can be used as a biomarker for the diagnosis of ovarian cancer.

Fig. 5 shows the accuracy and cross-entropy loss of the CNN ovarian cancer diagnostic model in a training dataset. As can be seen in Fig. 5, the accuracy of the model did not improve significantly after 800 training steps. The red curve represents the training accuracy of each batch of samples, and the final average accuracy of the model is 99.7%. The blue curve represents the value of cross-entropy loss during model training. The smaller the cross-entropy loss value is, the better the classification efficiency of the model. Finally, the final average cross-entropy

loss value of the model reaches 0.022. In addition, Fig. 6 shows the accuracy and cross-entropy loss of the CNN model for diagnosing ovarian cancer in the validation dataset, where the final average validation accuracy and loss of the model reached 99.42% and 0.015, respectively. Thus, these results demonstrate that the CNN model for diagnosing ovarian cancer constructed by transfer learning on the ResNet50 architecture is capable of identifying freshly isolated ovarian tissues (benign, malignant, normal) without additional tissue processing.

After the training of the CNN ovarian cancer diagnostic model was completed, the test dataset was used to check the generalization ability of the constructed model. Fig. 7 shows in the form of a confusion matrix, the differences between the true and predicted classes obtained by the CNN ovarian cancer diagnostic model on the test dataset. Among them, 100% of benign samples, 100% of malignant samples and 99.7% of normal samples were correctly predicted. Unfortunately, 0.3% of normal samples were misdiagnosed as benign samples. In addition, the t-SNE (t-distributed Stochastic Neighbor Embedding) was used to investigate the internal features learned from the CNN model for ovarian cancer diagnosis (Fig. 8) [39]. As shown in Fig. 8, each point represents an SHG image of the ovary projected in two dimensions from the output of the SoftMax layer in the CNN ovarian cancer diagnostic model. It can be seen that the points of the same ovarian tissue type are most clustered together (Fig. 8, insets show representative images of different diseases). These results show that the CNN ovarian cancer diagnostic model proposed in this experiment has good generalization ability.

IV. DISCUSSION

Collagen is the basic skeleton of tissue matrix and plays an important role in tumor formation and development. In particular, with the progression of ovarian tissue deterioration, the collagen composition in the extracellular matrix exhibits varying degrees of change [40]. Therefore, the rapid and accurate examination of collagen components in ovarian tissues in this study provides a method for diagnosing tumor progression. Although X-rays, MRI, and other imaging methods commonly used in clinical practice can detect collagen components, their image resolution is relatively low (on the order of millimeters) in detecting

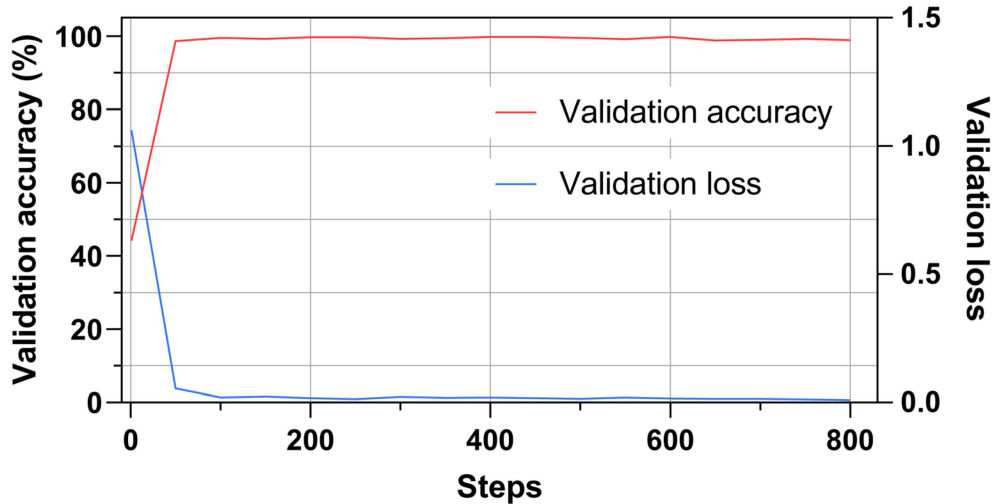


Fig. 6. Training performance of the CNN ovarian cancer diagnosis model in the validation dataset.

		True class				
		Benign	Malignant	Normal		
True class	Benign	902	0	0	100.0%	
	Malignant	0	902	0	100.0%	
Normal	Benign	3	0	899	99.7%	0.3%
	Predicted class	True Positive		False Negative		

Fig. 7. Confusion matrix of the CNN ovarian cancer diagnostic model in the test dataset.

small changes [41], [42]. In addition, the ionizing radiation generated during imaging can be detrimental to human health. Finally, the histopathological examination is also required for a definitive diagnosis. As shown in Fig. 1, the conventional histopathological analysis method is time-consuming and may cause inter-observer bias. Therefore, there is an urgent need to develop a rapid, non-destructive and accurate model for diagnosing ovarian cancer that can assist physicians in evaluating surgical specimens' and improve surgical outcomes and patient prognosis.

In this study, SHG imaging technology was used to obtain high-resolution collagen images of freshly excised ovarian tissue without staining. In addition, a CNN model was created to diagnose ovarian cancer by modifying the ResNet50 network

through transfer learning. This model successfully identified benign, malignant, and normal ovarian tissue with an average accuracy of 99.7%. Unlike histopathological analysis, SHG imaging does not require any special processing of the ovarian tissue, such as fixation, dehydration, embedding, sectioning and staining. It takes only a few seconds to obtain a SHG image with a pixel size of 512×512 ($134.95 \mu\text{m} \times 134.95 \mu\text{m}$). Compared with the conventional histopathological analysis method, the acquisition time for SHG images containing collagen information in ovarian tissue is significantly shorter. In addition, SHG imaging technology greatly reduces tissue damage caused by tissue processing artifacts in histopathological examination, which lays a foundation for rapid diagnosis of ovarian cancer in surgery. To further advance the rapid, accurate and automatic

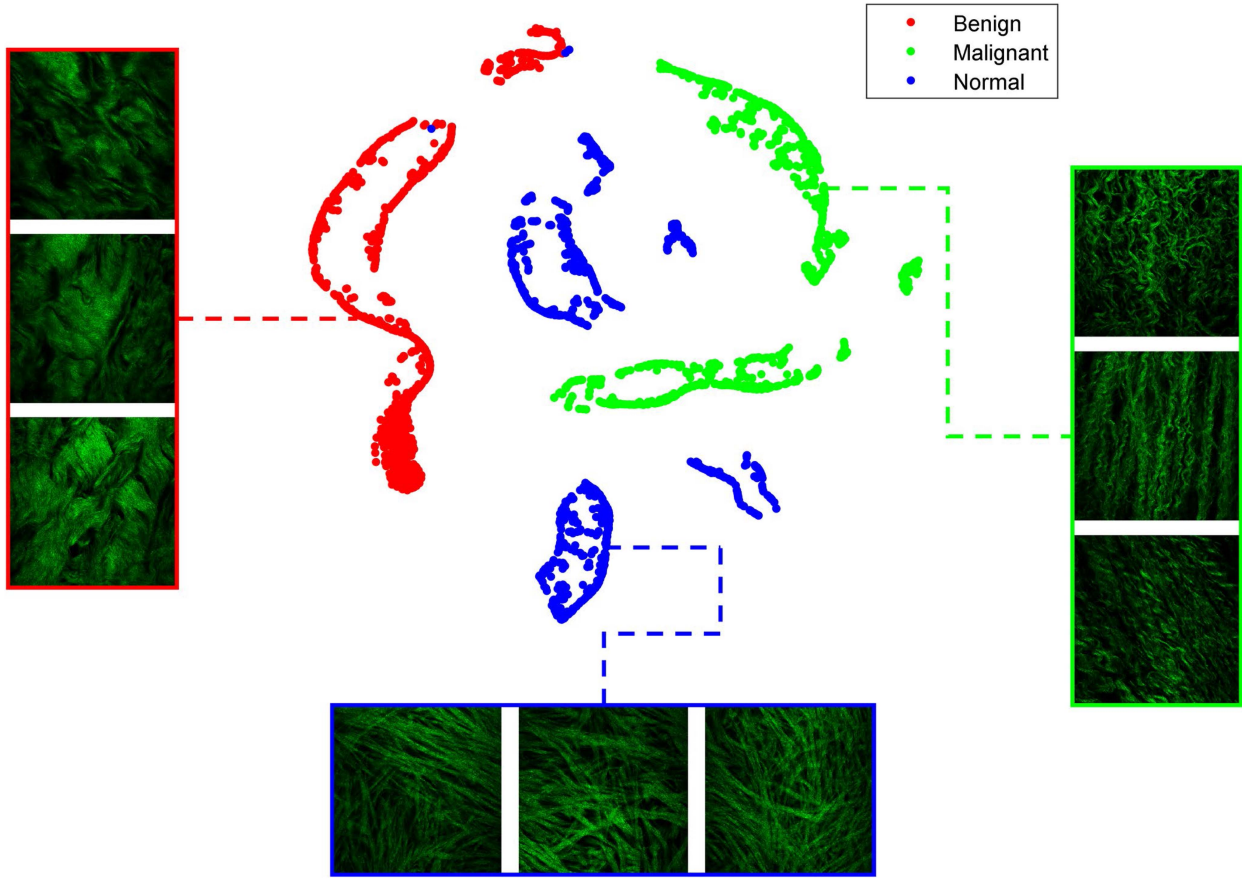


Fig. 8. t-SNE visualization of the output of SoftMax layer in the CNN ovarian cancer diagnostic model for the identification of three different ovarian tissue types in the test dataset. Colored point clouds represent the different disease categories (red: Benign, green: Malignant, blue: Normal). The insets show the representative SHG images of the corresponding ovarian tissue types.

diagnosis of ovarian cancer based on SHG images, CNN was used in this study to identify different ovarian tissue types by transfer learning. Compared with conventional diagnosis by pathologists, it can objectively learn and classify related features in SHG images, reduce inter-observer errors caused by subjective factors during histopathological analysis, and improve work efficiency. Therefore, the CNN ovarian cancer diagnostic model, combining the label-free SHG imaging technology and the CNN image classification algorithm, can effectively provide the rapid, non-destructive, accurate, and automatic ovarian cancer diagnosis, demonstrating its immense value for the rapid and accurate intraoperative diagnosis. Besides, the end-to-end deep learning method proposed in this work was superior to the traditional feature extraction combined with machine learning methods in many aspects. Previously, our research group proposed a computer-aided diagnosis model of ovarian cancer based on radiomics feature extraction method combined with automated machine learning tree-based pipeline optimization tool (Radiomics-TPOT), with an accuracy of more than 90% [28]. To further compare the performance of each method, they are applied to the same data set for comparison experiment. The results are shown in Table I. It can be seen that the accuracy of deep learning method is better than that of feature extraction combined with traditional machine learning method.

TABLE I
CLASSIFICATION ACCURACY COMPARISON BETWEEN CONVENTIONAL
MACHINE LEARNING AND DEEP LEARNING IN THE SAME DATASET

	Radiomics-TPOT	Modified CNN
Accuracy	90.8%	99.7%
SD	±0.9	±0.2

Radiomics-TPOT=radiomics feature extraction combined with tree-based pipeline optimization tool (TPOT), CNN= Convolutional neural networks.

This mainly reflects that deep learning uses end-to-end training mode to process datasets, avoids excessive manual intervention, and improves the fitting of computer-aided diagnosis model. In addition, according our previous work [43], the collagen distribution at different depth is heterogeneous in ovarian tissues. Thus, in order to verify the depth dependence of CNN ovarian cancer diagnostic model provided in this study, ovarian tissue SHG images at different depths ($10\ \mu\text{m}$, $30\ \mu\text{m}$) were transmitted to this model. The classification results were shown in Table II. Although the image at different depths of the same sample shows different distribution, the collagen exhibits the same characteristics in the same tissue type. Therefore, the ovarian cancer diagnostic model learned the main differences among them. And this model still can accurately identify different ovarian tissues.

TABLE II
OVARIAN TISSUE DIAGNOSIS BASED ON SHG IMAGES AT 10 μm AND 30 μm

	10 μm	30 μm
Accuracy	92.7%	93.4%
SD	± 0.4	± 0.3

Furthermore, the method proposed in this study can be applied to other diseases associated with extracellular matrix remodeling.

Although the proposed model achieved good results in this study, it still has some limitations, such as: first, it is noted that 0.3% of normal samples were misclassified as benign when the trained model was run on the test dataset. The possible reason is that the training samples are relatively small, and additional datasets or information need to be introduced for a more comprehensive description. Second, because the ResNet50 network framework requires an input image size of 224×224 , this experiment used the down-sampling method to adjust the size of the 512×512 SHG images, which may result in a loss of collagen structure details and texture information, which can affect the final classification result and lead to the misjudgment of the image category. Therefore, this study will consider the following work in future research to improve the performance of the proposed model: First, introduce a three-dimensional SHG deep learning image model to analyze the collagen changes more comprehensively as ovarian cancer progresses, and then collect more samples to evaluate the model performance in multiple centers. In addition, you can expand the amount of information available in ovarian cancer diagnosis by combining the SHG signal with other biological tissue endogenous signals, such as two-photon fluorescence, three photon fluorescence, and third harmonic generation imaging (THG). Second, under the condition that the original resolution and identifiable information of the image are preserved, the size of the SHG image is adjusted by more proper resizing method such as random crop to meet the requirements of the deep learning network framework.

IV. CONCLUSION

In conclusion, this study successfully developed a CNN ovarian cancer diagnostic model for identifying freshly excised benign, malignant and normal ovarian tissues by combining SHG imaging technology with a deep learning image classification algorithm, to achieve rapid, non-destructive, accurate and automatic diagnosis of ovarian cancer with an average classification accuracy of 99.7%. The proposed model can effectively assist doctors in rapid and accurate classification of intraoperative patients, provide valuable information for determining of the size of surgical excision, and improve the efficiency of diagnosis in surgery.

ACKNOWLEDGMENT

The authors would like to thank Bingham Chen for artwork on Fig. 3. The authors would also like to thank Prof. Chenyuan Dong for his valuable suggestions.

REFERENCES

- [1] P. Gaona-Luviano, L. A. Medina-Gaona, and K. Magaña-Pérez, "Epidemiology of ovarian cancer," *Chin. Clin. Oncol.*, vol. 9, no. 4, pp. 47–54, 2020.
- [2] M. C. Haffner, A. M. De Marzo, S. Yegnasubramanian, J. I. Epstein, and H. B. Carter, "Diagnostic challenges of clonal heterogeneity in prostate cancer," *J. Clin. Oncol.*, vol. 33, no. 7, pp. e38–e40, 2015.
- [3] T. M. Ripping, K. T. Haaf, A. L. Verbeek, N. T. van Ravesteyn, and M. J. Broeders, "Quantifying overdiagnosis in cancer screening: A systematic review to evaluate the methodology," *JNCI: J. Nat. Cancer Inst.*, vol. 109, no. 10, 2017, Art. no. ddx060.
- [4] H. A. Altirkistani, F. M. Tashkandi, and Z. M. Mohammedsahle, "Histological stains: A literature review and case study," *Glob. J. Health Sci.*, vol. 8, no. 3, pp. 72–79, 2016.
- [5] M. Titford and B. Bowman, "What may the future hold for histotechnologists?", *Lab. Med.*, vol. 43, no. 2, pp. e5–e10, 2012.
- [6] R. J. Buesa, "Histology: A unique area of the medical laboratory," *Ann. Diagn. Pathol.*, vol. 11, no. 2, pp. 137–141, 2007.
- [7] J. B. Osborn, G. L. Keeney, J. W. Jakub, A. C. Degnim, and J. C. Boughey, "Cost-effectiveness analysis of routine frozen-section analysis of breast margins compared with reoperation for positive margins," *Ann. Surg. Oncol.*, vol. 18, no. 11, pp. 3204–3209, 2011.
- [8] F. J. Voskuil et al., "Intraoperative imaging in pathology-assisted surgery," *Nature Biomed. Eng.*, vol. 6, no. 5, pp. 503–514, May 2022.
- [9] J. Pallud et al., "Long-term results of carbamustine wafer implantation for newly diagnosed glioblastomas: A controlled propensity-matched analysis of a French multicenter cohort," *Neuro-Oncol.*, vol. 17, no. 12, pp. 1609–1619, 2015.
- [10] T. Nowikiewicz et al., "Clinical outcomes of an intraoperative surgical margin assessment using the fresh frozen section method in patients with invasive breast cancer undergoing breast-conserving surgery—a single center analysis," *Sci. Rep.*, vol. 9, no. 1, pp. 1–8, 2019.
- [11] K. J. Chambers, S. Kraft, and K. Emerick, "Evaluation of frozen section margins in high-risk cutaneous squamous cell carcinomas of the head and neck," *Laryngoscope*, vol. 125, no. 3, pp. 636–639, 2015.
- [12] E. R. S. John et al., "Diagnostic accuracy of intraoperative techniques for margin assessment in breast cancer surgery," *Ann. Surg.*, vol. 265, no. 2, pp. 300–310, 2017.
- [13] E. Mahe et al., "Intraoperative pathology consultation: Error, cause and impact," *Can. J. Surg.*, vol. 56, no. 3, pp. E13–E18, 2013.
- [14] P. J. Campagnola and L. M. Loew, "Second-harmonic imaging microscopy for visualizing biomolecular arrays in cells, tissues and organisms," *Nature Biotechnol.*, vol. 21, no. 11, pp. 1356–1360, 2003.
- [15] P. J. Campagnola, H. A. Clark, W. A. Mohler, A. Lewis, and L. M. Loew, "Second harmonic imaging microscopy of living cells," *J. Biomed. Opt.*, vol. 6, no. 3, pp. 277–286, 2001.
- [16] V. Ajeti et al., "Structural changes in mixed Col I/Col V collagen gels probed by SHG microscopy: Implications for probing stromal alterations in human breast cancer," *Biomed. Opt. Exp.*, vol. 2, no. 8, pp. 2307–2316, 2011.
- [17] L. Mostaço-Guidolin, N. L. Rosin, and T.-L. Hackett, "Imaging collagen in scar tissue: Developments in second harmonic generation microscopy for biomedical applications," *Int. J. Mol. Sci.*, vol. 18, no. 8, 2017, Art. no. 1772.
- [18] P. Campagnola, "Second harmonic generation imaging microscopy: Applications to diseases diagnostics," *Anal. Chem.*, vol. 83, no. 9, pp. 3224–3231, 2011.
- [19] C. Bonnans, J. Chou, and Z. Werb, "Remodelling the extracellular matrix in development and disease," *Nature Rev. Mol. Cell Biol.*, vol. 15, no. 12, pp. 786–801, 2014.
- [20] P. P. Provenzano et al., "Collagen density promotes mammary tumor initiation and progression," *BMC Med.*, vol. 6, no. 1, pp. 1–15, 2008.
- [21] T. R. Cox and J. T. Erler, "Remodeling and homeostasis of the extracellular matrix: Implications for fibrotic diseases and cancer," *Dis. Models Mechanisms*, vol. 4, no. 2, pp. 165–178, 2011.
- [22] P. Mobadersany et al., "Predicting cancer outcomes from histology and genomics using convolutional networks," *Proc. Nat. Acad. Sci.*, vol. 115, no. 13, pp. E2970–E2979, 2018.
- [23] N. Coudray et al., "Classification and mutation prediction from non-small cell lung cancer histopathology images using deep learning," *Nature Med.*, vol. 24, no. 10, pp. 1559–1567, 2018.
- [24] K. Doi, "Computer-aided diagnosis in medical imaging: Historical review, current status and future potential," *Computerized Med. Imag. Graph.*, vol. 31, no. 4/5, pp. 198–211, 2007.

- [25] J. R. F. Junior, M. Koenigkam-Santos, F. E. G. Cipriano, A. T. Fabro, and P. M. de Azevedo-Marques, "Radiomics-based features for pattern recognition of lung cancer histopathology and metastases," *Comput. Methods Prog. Biomed.*, vol. 159, pp. 23–30, 2018.
- [26] E. M. El Houby, "A survey on applying machine learning techniques for management of diseases," *J. Appl. Biomed.*, vol. 16, no. 3, pp. 165–174, 2018.
- [27] J. Torrents-Barrena, D. Puig, J. Melendez, and A. Valls, "Computer-aided diagnosis of breast cancer via Gabor wavelet bank and binary-class SVM in mammographic images," *J. Exp. Theor. Artif. Intell.*, vol. 28, no. 1/2, pp. 295–311, 2016.
- [28] G. Wang et al., "Rapid identification of human ovarian cancer in second harmonic generation images using radiomics feature analyses and tree-based pipeline optimization tool," *J. Biophotonics*, vol. 13, no. 9, 2020, Art. no. e202000050.
- [29] G. Wang et al., "Machine learning-based rapid diagnosis of human borderline ovarian cancer on second-harmonic generation images," *Biomed. Opt. Exp.*, vol. 12, no. 9, pp. 5658–5669, 2021.
- [30] A. Krizhevsky, I. Sutskever, and G. E. Hinton, "Imagenet classification with deep convolutional neural networks," in *Proc. 25th Int. Conf. Neural Inf. Process. Syst.*, vol. 25, 2012, pp. 1097–1105.
- [31] S. Pereira, A. Pinto, V. Alves, and C. A. Silva, "Brain tumor segmentation using convolutional neural networks in MRI images," *IEEE Trans. Med. Imag.*, vol. 35, no. 5, pp. 1240–1251, May 2016.
- [32] K. Kamnitsas et al., "Efficient multi-scale 3D CNN with fully connected CRF for accurate brain lesion segmentation," *Med. Image Anal.*, vol. 36, pp. 61–78, 2017.
- [33] A. Esteva et al., "Dermatologist-level classification of skin cancer with deep neural networks," *Nature*, vol. 542, no. 7639, pp. 115–118, 2017.
- [34] R. Yang and Y. Yu, "Artificial convolutional neural network in object detection and semantic segmentation for medical imaging analysis," *Front. Oncol.*, vol. 11, 2021, Art. no. 638182.
- [35] M. Kim et al., "Deep learning in medical imaging," *Neurospine*, vol. 16, no. 4, 2019, Art. no. 657.
- [36] O. Russakovsky et al., "Imagenet large scale visual recognition challenge," *Int. J. Comput. Vis.*, vol. 115, no. 3, pp. 211–252, 2015.
- [37] K. He, X. Zhang, S. Ren, and J. Sun, "Deep residual learning for image recognition," in *Proc. IEEE Conf. Comput. Vis. Pattern Recognit.*, 2016, pp. 770–778.
- [38] K. Weiss, T. M. Khoshgoftaar, and D. Wang, "A survey of transfer learning," *J. Big Data*, vol. 3, no. 1, pp. 1–40, 2016.
- [39] L. Van der Maaten and G. Hinton, "Visualizing data using t-SNE," *J. Mach. Learn. Res.*, vol. 9, no. 11, 2008, pp. 2579–2605.
- [40] S. Alkmin et al., "Role of collagen fiber morphology on ovarian cancer cell migration using image-based models of the extracellular matrix," *Cancers*, vol. 12, no. 6, 2020, Art. no. 1390.
- [41] N. Takeshita et al., "Bilateral ovarian fibromatosis diagnosed with magnetic resonance imaging: A case report," *Osaka City Med. J.*, vol. 65, no. 2, pp. 135–140, 2019.
- [42] M. J. Ceko, K. Hummitzsch, N. Hatzirodos, R. J. Rodgers, and H. H. Harris, "Quantitative elemental analysis of bovine ovarian follicles using X-ray fluorescence imaging," *Metallomics*, vol. 7, no. 5, pp. 828–836, 2015.
- [43] S. Qian et al., "Identification of human ovarian cancer relying on collagen fiber coverage features by quantitative second harmonic generation imaging," *Opt. Exp.*, vol. 30, no. 14, pp. 25718–25733, 2022.

Huiling Zhan received the B.S. degree in mathematics and applied mathematics from Putian University, Putian, China, in 2020. She is currently working toward the M.S. degree with the School of Science, Jimei University, Xiamen, China. Her research interests include the intelligent information processing and the development and applications of nonlinear optical microscopy in biological and biomedical research.

Tianyi Luo received the B.S. degree in mathematics and applied mathematics from Jimei University, Xiamen, China, in 2021. She is working toward the M.S. degree with the School of Science, Jimei University. Her research interests include the intelligent information processing and the development and applications of nonlinear optical microscopy in biological and biomedical research.

Bingzi Kang received the B.S. degree in mathematics and applied mathematics from Henan Normal University, Xinxiang, China, in 2022. She is currently working toward the M.S. degree with the School of Science, Jimei University, Xiamen, China. Her research interests include the intelligent information processing and the development and biomedical imaging process.

Xiaolu Li received the Ph.D. degree in optics engineering from the Shanghai Institute of Optics and Fine Mechanics, Chinese Academy of Sciences, Beijing, China, in 2020. She is currently a Lecturer with the School of Science, Jimei University, Xiamen, China. Her research interests include the development and applications of nonlinear optical microscopy in biological and biomedical research.

Gangqin Xi received the Ph.D. degree in optics engineering from Fujian Normal University, Fuzhou, China, in 2021. She is currently a Lecturer with the School of Science, Jimei University, Xiamen, China. Her research interests include the development and applications of nonlinear optical microscopy in biological and biomedical research.

Zhiyi Liu received the B.S. degree in optical information science and technology from the Minzu University of China, Beijing, China, in 2007, and the Ph.D. degree in physics from Tsinghua University, Beijing, China, in 2013. From 2013 to 2018, he had Postdoctoral training with Georgakoudi Lab, Tufts University, Boston, MA, USA. He is currently a ZJU100 Young Professor with the College of Optical Science and Engineering, Zhejiang University, Hangzhou, China. He works on the biomedical imaging of tissues relying on endogenous contrast. By exploring the quantitative characteristics of both cells and extracellular matrix, he is trying to gain a better understanding of cell-matrix interactions during progression of diseases.

Shuangmu Zhuo received the Ph.D. degree in optics engineering from Fujian Normal University, Fuzhou, China, in 2012. He joined the Singapore-MIT Alliance for Research and Technology as a Postdoctoral Research Fellow. He is currently a Professor with the School of Science, Jimei University, Xiamen, China. His research interests include the development and applications of nonlinear optical microscopy in biological and biomedical research.

Guangxing Wang received the M.S. degree in optics engineering from Fujian Normal University, Fuzhou, China, in 2020. He is currently working toward the Ph.D. degree with the Center for Molecular Imaging and Translational Medicine School of Public Health, Xiamen University, Xiamen, China. He also cooperates with the School of Science, Jimei University, Xiamen. His research interests include the optogenetics and the development and applications of nonlinear optical microscopy in biological and biomedical research.